

<https://doi.org/10.1038/s42003-025-08006-x>

Preference-independent saliency map in the mouse superior colliculus

Check for updates

Ruixiang Wu¹, Jinhui Xu¹, Chunpeng Li^{1,2}, Zhaoji Zhang^{1,3}, Shu Lin^{1,2}, Ling-yun Li⁴ & Ya-tang Li¹ ✉

Detecting salient stimuli in a visual scene is crucial for animal survival, yet how the brain encodes visual saliency remains unclear. Here, using two-photon calcium imaging, we reveal a preference-independent saliency map in the superficial superior colliculus of awake mice. Salient stimuli evoke stronger responses than uniform stimuli in both excitatory and inhibitory neurons, with similar encoding patterns across both cell types. The strongest response occurs when a salient stimulus is centered within the receptive field, with contextual effects extending approximately 40°. Response amplitude scales with saliency strength but remains independent of neurons' orientation or motion direction preferences. Notably, saliency-encoding neurons exhibit weak orientation and direction selectivity, indicating a complementary relationship between saliency and feature maps. Importantly, this preference-independent saliency encoding does not require cortical inputs. These findings provide insights into the neural mechanisms underlying visual saliency detection.

Every second, humans extract about 20 bits of relevant information from the one gigabit of visual input entering the eyes to guide behavior^{1,2}. Visual attention is critical in filtering this vast influx of data, enabling survival in a complex and ever-changing environment. There are two types of visual attention: endogenous and exogenous. Endogenous attention is goal-directed, such as searching for a specific object in a scene. In contrast, exogenous attention is stimulus-driven and automatically directed towards salient objects that “pop out” in the visual scene^{3–7}.

Saliency, defined as the conspicuousness of a specific visual area within a scene, arises from physical attributes such as orientation, color, motion direction, size, and shape. Where and how visual saliency is encoded in the brain remains debated. A theoretical model proposes the existence of a feature-independent saliency map in the brain^{8,9}. This map integrates inputs from multiple feature maps to encode saliency strength regardless of feature preferences. It then merges with goal-driven attention to generate a priority map, ultimately guiding where to attend^{10,11}. In primates, several brain regions have been implicated in encoding visual saliency, including the primary visual cortex (V1)^{12–15}, the superficial and intermediate layers of the superior colliculus (sSC and iSC)¹⁶, V4¹⁷, the posterior parietal cortex¹⁸, and the frontal eye field¹⁹. However, except for sSC and V1, these regions also process goal-driven attention, suggesting they may inherit saliency maps from upstream regions and instead host priority maps²⁰.

Although the theory predicts that ideal saliency-encoding neurons respond to salient stimuli independently of their preferences within a

specific visual feature or across different features, experimental evidence from both V1 and sSC fails to consistently support this prediction. In cat and monkey V1, salient stimuli made by orientation have elicited larger, similar, or smaller responses compared to iso-orientation stimuli^{13,14,21–23}. Similar inconsistencies have been observed in responses to salient stimuli made by motion direction^{15,24,25}. These contradictory findings can be largely reconciled by considering neurons' orientation or direction preferences. A recent study in primate V1 found that responses to salient stimuli are influenced by both the orientation contrast of stimuli and neurons' orientation preferences¹³, contradicting the model prediction. Encoding of saliency in sSC is also debated. Recent work in awake monkeys suggests a correlation between neural activity and saliency strength, but the role of feature preference remains unsolved¹⁶. Studies in mice further complicate this picture, as saliency encoding appears to be influenced by anesthesia and depends on the specific visual features that define saliency^{26,27}. Other factors, such as cortical integrity and the number of neurons recorded, may also affect data interpretation.

Furthermore, the relationship between feature encoding and saliency encoding remains poorly understood. At the single-neuron level, no clear correlation has been observed between orientation or direction selectivity and responses to salient stimuli²². At the population level, while the functional organization of orientation and motion direction has been well-documented in the visual cortex across species^{28–32} and in the mouse SC^{33–36}, neither saliency maps nor their relationship to feature maps has been

¹Chinese Institute for Brain Research, Beijing (CIBR), Beijing, China. ²College of Biological Sciences, China Agricultural University, Beijing, China. ³College of Chemistry and Molecular Engineering, Peking University, Beijing, China. ⁴Department of Neurobiology, School of Basic Medical Sciences, Capital Medical University, Beijing, China. ✉e-mail: yatangli@cibr.ac.cn

reported. Because perceptually detecting saliency is orthogonal to detecting features, we hypothesize that neurons involved in feature encoding are less likely to encode visual saliency.

To test our hypothesis and investigate the neural encoding of visual saliency, we conducted *in vivo* two-photon calcium imaging in the sSC of awake head-fixed mice with an intact cortex. Our goal was to understand how the encoding of visual saliency is affected by different visual features and contributed by excitatory and inhibitory neurons across different depths of the sSC. To achieve this, we expressed non-floxed GCaMP8 in the mouse sSC, where GABAergic or glutamatergic neurons were genetically labeled by tdTomato. We then measured and analyzed neuronal responses to salient stimuli defined by orientation or motion direction. Our results provide the first direct experimental evidence supporting the existence of preference-independent saliency maps in the brain. Specifically, for both excitatory and inhibitory neurons in the mouse SC, the encoding of visual saliency is not influenced by their preference for specific orientations or motion directions. Furthermore, supporting our hypothesis, neurons involved in saliency encoding cluster together to form maps within the sSC and exhibit weaker tuning to orientation and motion direction.

Results

Excitatory and inhibitory neurons show robust responses to salient stimuli in the sSC of awake mice

To reveal how the sSC encodes visual saliency, we performed two-photon calcium imaging in the posterior-medial SC of awake head-fixed mice (Fig. 1a, b), leaving the cortex intact as previously described^{33,36,37}. We measured the activity of excitatory and inhibitory neurons in response to visually salient stimuli. Excitatory and inhibitory neurons were distinguished by expressing tdTomato in genetically labeled neurons in Vglut2-Cre or Vgat-Cre mice (Fig. 1c). In both lines, excitatory neurons comprised about 40% of the total population, consistent with the fluorescence *in situ* hybridization data³⁸. Across 54 imaging planes and up to a depth of 300 μm , we recorded a total of 3232 excitatory neurons and 5103 inhibitory neurons from eight animals. Throughout the imaging session, animals exhibited occasional locomotion and eye movements (Supplementary Fig. 1a, d). During locomotion, pupil size was positively correlated with locomotion speed, and neuronal responses showed either a negative or positive correlation with pupil size (Supplementary Fig. 1b, c), consistent with previous findings³⁹.

Presumably, saliency-encoding neurons should show stronger responses to salient stimuli than to uniform stimuli. To test this, we measured neuronal responses to stimuli in which saliency was defined by either orientation or motion direction. For orientation-defined saliency, we used salient flashing gratings (SFGs): a 10° patch grating superimposed on a full-field grating in the orthogonal orientation, both flashed simultaneously on a gray background (see Methods). We tested two stimulus configurations: circular patches with sinusoidal gratings and square patches with square gratings. In both cases, excitatory and inhibitory neurons showed stronger responses to salient stimuli when the salient patch was centered in their receptive fields (RFs) compared to responses to the background alone (Fig. 1d). For direction-defined saliency, we used salient moving gratings (SMGs): a 10° patch grating moving in one direction superimposed on a full-field grating moving in the opposite direction. Similarly, both types of neurons responded more strongly to SMGs compared to uniform stimuli (Fig. 1e). The enhanced responses to SFGs and SMGs suggest that the sSC plays an important role in encoding visual saliency. Because neuronal responses were consistent across circular and square patches, we combined the data for subsequent analysis.

Neural encoding of visual saliency is independent of orientation preference

Neurons in the sSC are retinotopically organized and show orientation preference. A neuron's response to SFGs is influenced by three factors: (1)

the distance between its RF center and the patch; (2) the orientation contrast between the patch and the background; and (3) its orientation preference. To understand how these three factors affect neuronal responses, we measured the RFs and orientation preferences of individual neurons, along with their responses to SFGs with the patch positioned at different spatial locations relative to their RFs. For both excitatory and inhibitory neurons, responses were strongest when the patch was centered in the RF and gradually decreased as the patch moved away (Fig. 2a, b and Supplementary Fig. 2a). These findings suggest that collicular neurons function as saliency detectors.

To disentangle the contributions of orientation contrast and neurons' orientation preferences, we grouped SFG-elicited neuronal responses based on whether the neurons preferred vertical or horizontal background gratings. Regardless of the background orientation, the response amplitude at the RF center remained constant for both types of neurons, indicating that saliency encoding in the sSC is independent of the orientation preference (Fig. 2c and Supplementary Fig. 2b–d). As the patch moved further from the RF center, the response amplitude gradually decreased, up to ~40°. For the preferred orientation, the response amplitude became comparable to that evoked by the background when the distance reached ~10°, the typical RF size of sSC neurons^{40,41}. A further decline in amplitude with increasing distance up to 40° suggests a long-range suppression effect from the patch. Conversely, a long-range facilitation effect was observed if the background grating was orthogonal to the neurons' preferred orientations. This contrasting long-range effect for preferred and orthogonal orientations could be mediated by local neurons with extended dendritic arbors, such as inhibitory horizontal cells and excitatory wide-field cells, which have dendrites extending up to 500 μm ⁴².

To confirm the preference-independent saliency encoding, we calculated a saliency index (SI) to quantify each neuron's contribution to saliency encoding (see Methods). For both excitatory and inhibitory neurons, about 80% showed stronger responses to salient stimuli compared to the background, even when the background matched their preferred orientation (Fig. 2d). Interestingly, a smaller proportion of saliency-encoding neurons exhibited orientation selectivity compared to non-saliency-encoding neurons (Fig. 2e), suggesting a negative correlation between saliency encoding and orientation selectivity. Among neurons encoding saliency (SI > 0), responses to SFGs remained consistent regardless of whether the background was aligned with or orthogonal to their preferred orientations, and this consistency was maintained even in highly orientation-selective neurons (Fig. 2f). Furthermore, the difference in responses to SFGs with different backgrounds was uncorrelated with the orientation selectivity index (OSI), supporting the notion of preference-independent saliency encoding. These findings remain robust when the SI was defined as the relative difference between responses to SFGs and those to flashing squares on a gray background (Supplementary Fig. 2e–g). Thus, our data demonstrate that saliency encoding in the sSC is independent of orientation preference for individual neurons. In addition, saliency encoding remained consistent across different depths within the sSC (Supplementary Fig. 3).

Neural encoding of visual saliency is independent of direction preference

Saliency in visual stimuli can be induced by different features. To explore whether the orientation preference-independent saliency encoding generalizes to other features, we measured and analyzed neuronal responses to SMGs. Consistent with SFG-evoked responses, neurons exhibited the strongest responses when the patch was centered in the RF, with the response amplitude decreasing as the patch moved away from the RF center (Fig. 3a, b). Further analysis revealed a negative correlation between visual saliency and motion direction encoding (Fig. 3c, d), mirroring what was observed for orientation. For neurons encoding both saliency and motion direction, response amplitude remained consistent regardless of whether the background moved in the preferred or null direction (Fig. 3e). Furthermore, the difference in responses to SMGs with the background moving in

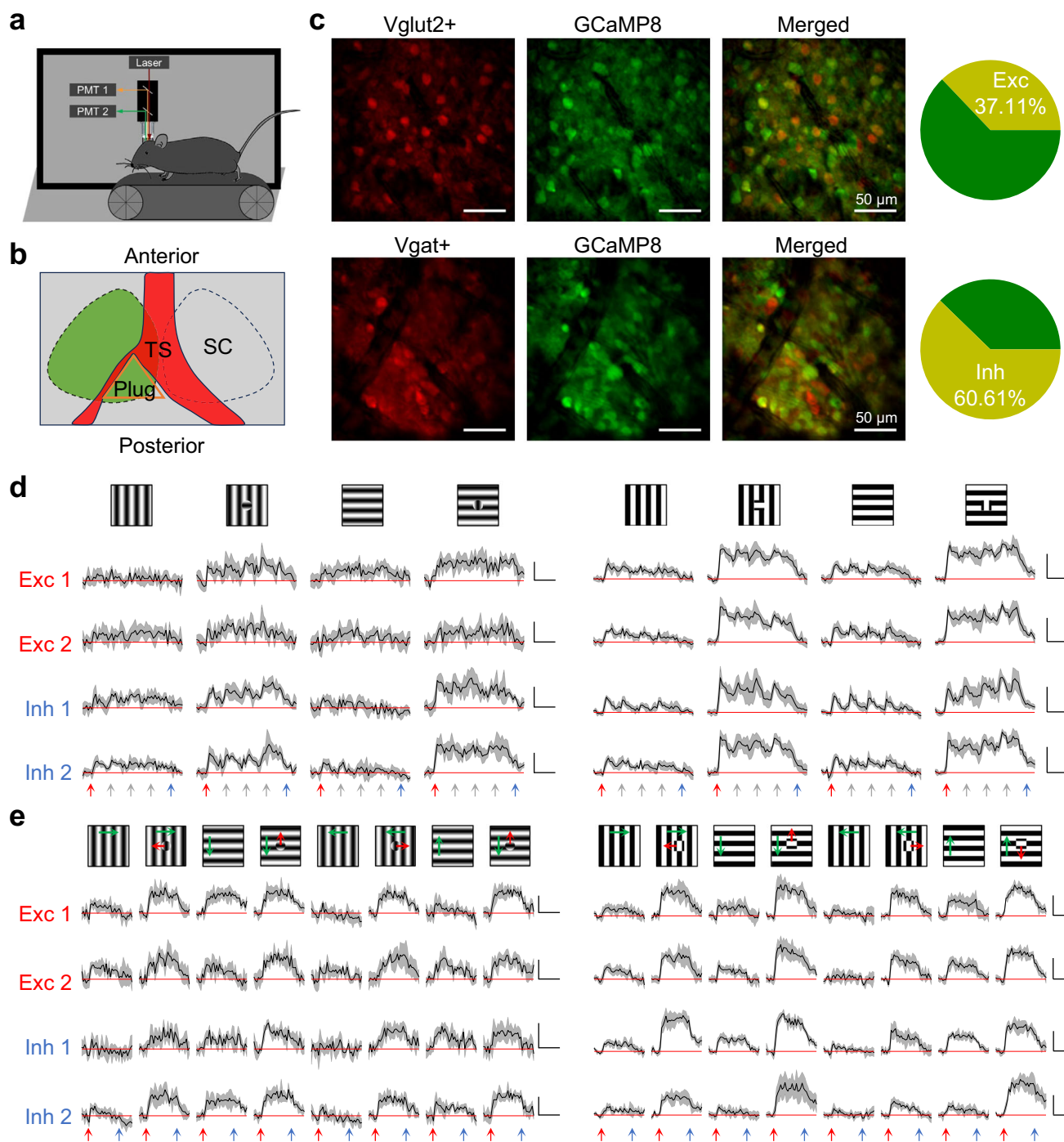


Fig. 1 | Excitatory and inhibitory neurons show robust responses to salient stimuli. **a** Schematic of the experimental setup. Mice were head-fixed and free to run on a treadmill. Visual stimuli were presented on a screen. Two-photon microscopy was used to image neuronal calcium activity and tdTomato expression. PMT, photomultiplier tube. **b** Schematic of mouse brain anatomy after insertion of a triangular transparent plug to expose the posterior-middle portion of the superior colliculus beneath the posterior cortex. TS, transverse sinus. **c** A mean projection of tdTomato-labeled Vglut2+ or Vgat+ neurons and GCaMP8+ neurons in two mice. The right panel shows the proportion of double-labeled neurons in both Vglut2-tdTomato and Vgat-tdTomato mice. **d** Example response profiles of excitatory and inhibitory

neurons to salient flashing gratings and backgrounds. Left, circular patches with sinusoidal gratings. Right, square patches with square gratings. Gray shade indicates the SD across 5 trials. Blue and red arrows mark the onset and offset of visual stimuli, respectively, while gray arrows mark the phase shift of the gratings. Red lines indicate the baseline activity without visual stimulation. Scale: 30% $\Delta F/F_0$, 0.5 s. **e** Example response profiles to salient moving gratings and backgrounds. Gray shade indicates the SD across 5 trials. Blue and red arrows mark the onset and offset of visual stimuli, respectively. Red lines indicate the baseline activity without visual stimulation. Scale: 30% $\Delta F/F_0$, 0.5 s.

opposite directions showed no correlation with the direction selectivity index (DSI). Taken together, these findings demonstrate that the encoding of visual saliency is independent of a neuron’s preference for both orientation and motion direction.

Neurons in the sSC encode saliency strength

An ideal saliency-encoding neuron would not only be independent of orientation and direction preference, but its amplitude would also reflect exclusively the saliency strength of visual stimuli. To examine whether

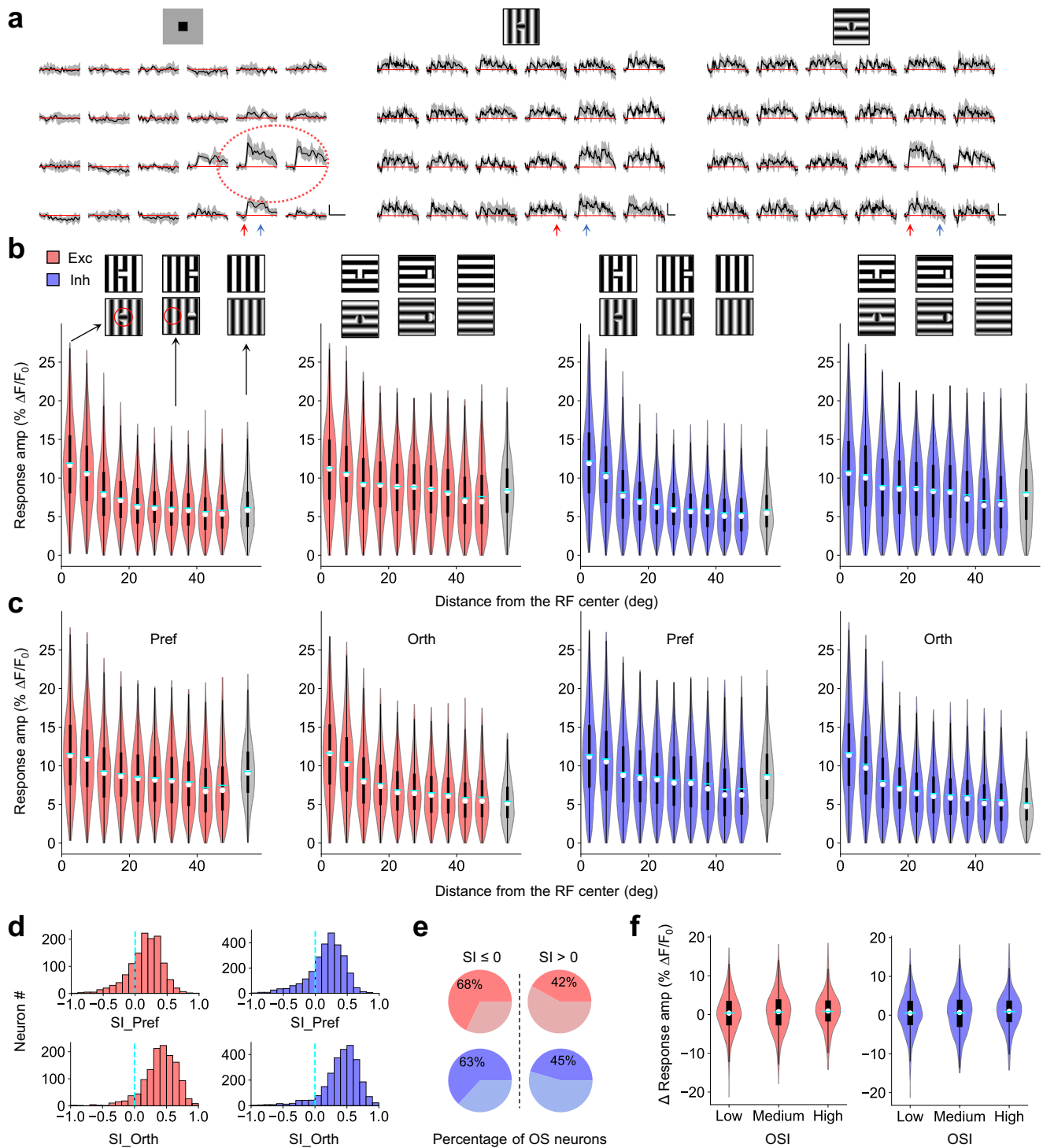


Fig. 2 | Neural encoding of visual saliency is independent of orientation preference. **a** Calcium responses of an example neuron to three types of visual stimuli: a flashing black square (10°) against a gray background (left), a flashing circular patch (10°) with horizontal (middle) or vertical (right) sinusoidal gratings against an orthogonal background. The patches were displayed at each of the 4 × 6 locations. Gray shade indicates the SD across 5 trials. Blue and red arrows mark the onset and offset of visual stimuli, respectively. The red dashed ellipse represents the outline of the fitted RF with a 2D Gaussian at half maximum. Red lines indicate the baseline activity without visual stimulation. Scale: 30% $\Delta F/F_0$, 1 s. **b** Violin plots for response amplitudes to SFGs with the patch at different distances from the RF center (colored bars), as well as amplitudes to the background (gray bars) for both excitatory (N = 1531) and inhibitory (N = 2915) neurons. Red circles denote the RF. **c** Response

amplitude to SFGs and backgrounds, grouped by the orientation preference of the background. **d** Histograms of SI for excitatory (Pref: 0.15 ± 0.26 ; Orth: 0.39 ± 0.26) and inhibitory (Pref: 0.17 ± 0.28 ; Orth: 0.41 ± 0.29) neurons. Cyan dashed lines mark the 0. **e** The percentage of orientation-selective neurons (OSI ≥ 0.25) in both non-saliency-encoding (SI ≤ 0 , left) and saliency-encoding (SI > 0 , right) populations. **f** Violin plots for the difference in response amplitudes evoked by SFGs with the preferred and orthogonal backgrounds for saliency-encoding neurons, plotted against different levels of orientation selectivity. Low: OSI < 0.25 ; Medium: $0.25 \leq$ OSI < 0.5 ; High: OSI ≥ 0.5 . The means of the three groups are the same: one-way ANOVA, $p = 0.15$ for excitatory neurons, N = 637, 309, 98; $p = 0.44$ for inhibitory neurons, N = 1087, 698, 160.

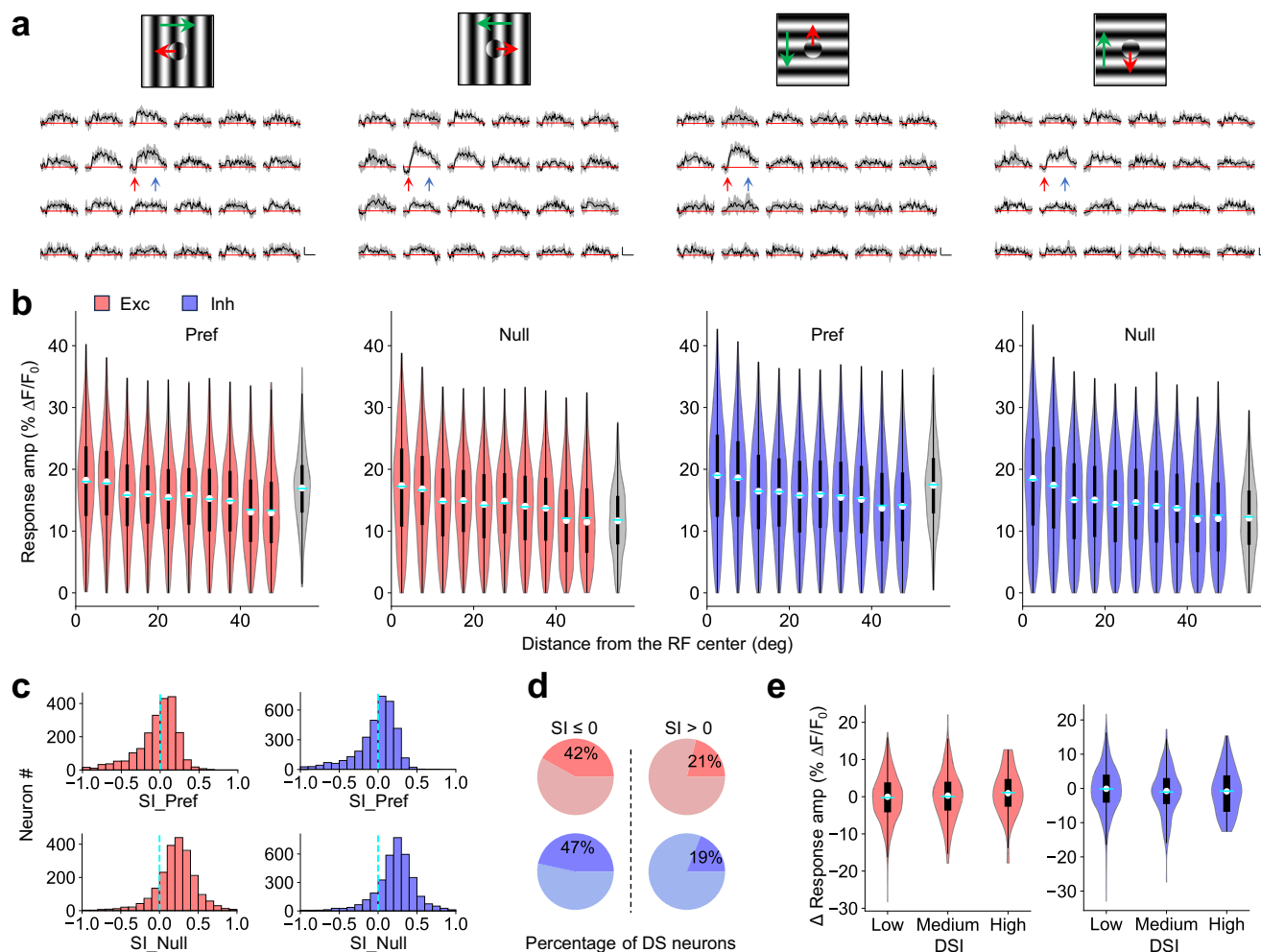


Fig. 3 | Neural encoding of visual saliency is independent of direction preference.

a Calcium responses of an example neuron to a circular patch (10°) sinusoidal grating moving in four directions against a background moving in the opposite direction. Green arrows indicate the motion direction of the background, and red arrows indicate the direction of the patch. Gray shade indicates the SD across 5 trials. Blue and red arrows mark the onset and offset of visual stimuli, respectively. Red lines indicate the baseline activity without visual stimulation. Scale: $30\% \Delta F/F_0$, 1 s. **b** Violin plots for response amplitudes to SMGs (colored bars) and the background (gray bars) for both excitatory ($N = 2082$) and inhibitory ($N = 3496$) neurons, grouped by direction preference. **c** Histograms of SI calculated from SMG-evoked

responses for excitatory (Pref: -0.03 ± 0.26 ; Null: 0.21 ± 0.25) and inhibitory (Pref: -0.02 ± 0.26 ; Null: 0.22 ± 0.25) neurons. Cyan dashed lines mark the 0. **d** The percentage of direction-selective neurons ($DSI \geq 0.25$) in both non-saliency-encoding ($SI \leq 0$, left) and saliency-encoding ($SI > 0$, right) populations. **e** Violin plots for the difference in response amplitudes evoked by SMGs with backgrounds moving in the preferred and null directions for saliency-encoding neurons, plotted against different levels of direction selectivity. Low: $DSI < 0.25$; Medium: $0.25 \leq DSI < 0.5$; High: $DSI \geq 0.5$. The means of the three groups are the same: one-way ANOVA, $p = 0.44$ for excitatory neurons, $N = 907, 197, 32$; $p = 0.10$ for inhibitory neurons, $N = 1555, 286, 58$.

neurons in the sSC meet this criterion, we systematically varied the patch's orientation against a fixed vertical or horizontal background, with an orientation contrast of 90° indicating the maximal saliency strength. Our results showed that neuronal responses indeed reflected the orientation contrast (Fig. 4a). To quantify the impact of orientation contrast, we examined the relationship between neuronal responses and orientation contrast in both excitatory and inhibitory neurons. The response amplitude of saliency-encoding neurons gradually decreased as the orientation contrast deviates from 90° , indicating that these neurons encode the saliency strength (Fig. 4b, d). Note that neuronal responses to salient stimuli with weak orientation contrasts could be smaller compared to responses to the preferred orientations. In particular, salient stimuli with 0° or 30° orientation contrast elicited weaker responses compared to the uniform stimuli at the preferred orientation (Supplementary Fig. 6a, b). Furthermore, the difference in response amplitude between 30° and 90° orientation contrasts reflected the difference in their saliency strength and was independent of the neuron's orientation selectivity (Fig. 4c, e).

Encoding of visual saliency depends on the preference across different visual features

So far, we have demonstrated that the response amplitude of saliency-encoding neurons correlates with the saliency strength of visual stimuli while remaining independent of their orientation or direction preferences. The theoretic model further predicts that the response amplitude of neurons should also be independent of their selectivity for various visual features that create saliency (Fig. 5a). Note that while the saliency strength of SFGs can be quantified as orientation contrast, it is challenging to directly compare the saliency strength between SFGs and SMGs. Ideally, the difference in response amplitude (ΔR) elicited by two salient stimuli would depend solely on the difference in their salient strength, independent of the neurons' preference for specific orientations, motion directions, or features (Fig. 5b). For example, ΔR between two stimuli with the same saliency strength should be close to zero and independent of OSI or DSI (Figs. 2f and 3e, orange line in Fig. 5b). When the saliency strength of two stimuli differs, ΔR should be non-zero and reflect this difference. This applies to salient stimuli made by the same feature (Fig. 4c, e, the green line in Fig. 5b) and by different

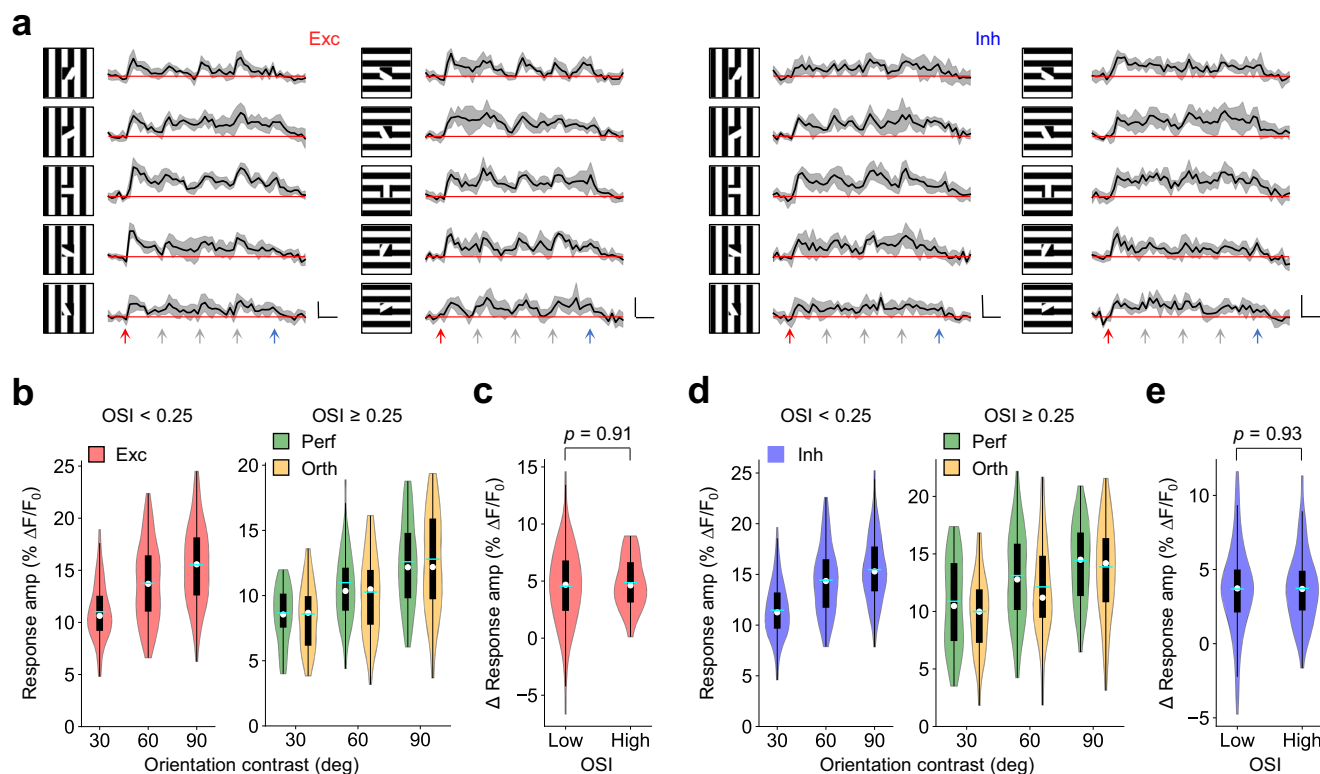


Fig. 4 | Neurons in the sSC encode saliency strength. **a** Response profiles of example excitatory and inhibitory neurons to SFGs with 5 different orientation contrasts in two backgrounds. Gray shade indicates the SD across 5 trials. Blue and red arrows mark the onset and offset of visual stimuli, respectively, while gray arrows mark the phase shift of the gratings. Red lines indicate the baseline activity without visual stimulation. Scale: 30% $\Delta F/F_0$, 0.5 s. **b** Violin plots for response amplitudes to

different orientation contrasts for saliency-encoding neurons with OSI < 0.25 (left, $N = 101$) and OSI ≥ 0.25 (right, $N = 37$). **c** Violin plots for the difference in response amplitudes elicited by SFGs of 30° and 90° contrasts for saliency-encoding neurons, plotted against different levels of orientation selectivity. Low: OSI < 0.25; High: OSI ≥ 0.25 , t -test. **d, e** The same plots for inhibitory neurons. Left, $N = 121$; Right, $N = 53$.

features (the blue line in Fig. 5b). To test whether saliency encoding is independent of feature selectivity, we compared neuronal responses evoked by SFGs and SMGs. The selectivity strength was quantified with a feature selectivity index (FSI, see Methods). Notably, our data revealed a strong positive correlation between FSI and ΔR (Fig. 5c). When neurons were divided into three groups with different levels of feature selectivity, ΔR varied significantly among groups (Fig. 5d). Thus, our results demonstrate that neural encoding of visual saliency is influenced by feature selectivity, contradicting the theoretic prediction. In addition, we observed a weak but significant positive correlation between SI_SFG and SI_SMG (Fig. 5e), suggesting some overlaps in neurons encoding saliency induced by orientation and motion direction.

Relationship between saliency map and feature map

Neurons tuned to orientation and motion direction form a functional map in the mouse SC^{33–36}. How does this feature encoding relate to saliency encoding? As shown in Figs. 2e and 3d, saliency-encoding neurons contain a smaller proportion of neurons selective for orientation or motion direction. To have a more comprehensive understanding of their relationship, we plotted the orientation map, direction map, and saliency maps for the same group of neurons (Fig. 6a). In the saliency map, neural encoding of saliency strength at different locations is indicated by SI. We found that neurons with strong orientation or direction selectivity tended to have low SI and show weak responses to salient stimuli (Fig. 6a and Supplementary Fig. 7a–c). To quantify the spatial organization of saliency encoding, we calculated the absolute difference in SI between neuron pairs as a function of their horizontal distance. This difference increased with distance up to approximately 100 μm , after which it stabilized (Fig. 6b), suggesting saliency-encoding neurons form patches with a radius of around 100 μm .

Further analysis revealed a significant negative correlation between SI and both gOSI and gDSI for excitatory and inhibitory neurons (Fig. 6c, d). This weak but significant negative correlation suggests that visual features and saliency are encoded by partially overlapping neural ensembles. This negative correlation can not be attributed to the response amplitude at the preferred orientation or direction, as feature selectivity is primarily driven by a decrease in responses at the orthogonal orientation or null direction (Supplementary Fig. 7d, e). Note that the saliency map described here differs from the one proposed in the theoretical model. In the model, the saliency map represents saliency strength at each location in the visual field. In contrast, the saliency map described here, similar to previously reported orientation and direction maps, represents the encoding capacity for visual saliency in anatomical space.

Preference-independent saliency encoding in the sSC does not require cortical inputs

Neurons in the sSC receive direct inputs from V1⁴³. To investigate how this top-down projection influences preference-independent saliency encoding in the sSC, we silenced V1 using muscimol, a GABA_A receptor agonist. Following drug injection, visually evoked responses in cortical neurons were largely suppressed (Fig. 7a). We then compared the responses of SC neurons to SFGs with different backgrounds after cortical silencing. For saliency-encoding neurons, responses to SFGs were unaffected by whether the background matched their preferred orientations (Fig. 7b), indicating that cortical inputs are not necessary for preference-independent saliency encoding in the sSC. Furthermore, after cortical silencing, the SI increased for both excitatory and inhibitory neurons (Fig. 7c), consistent with a previous study using electrophysiology²⁷.

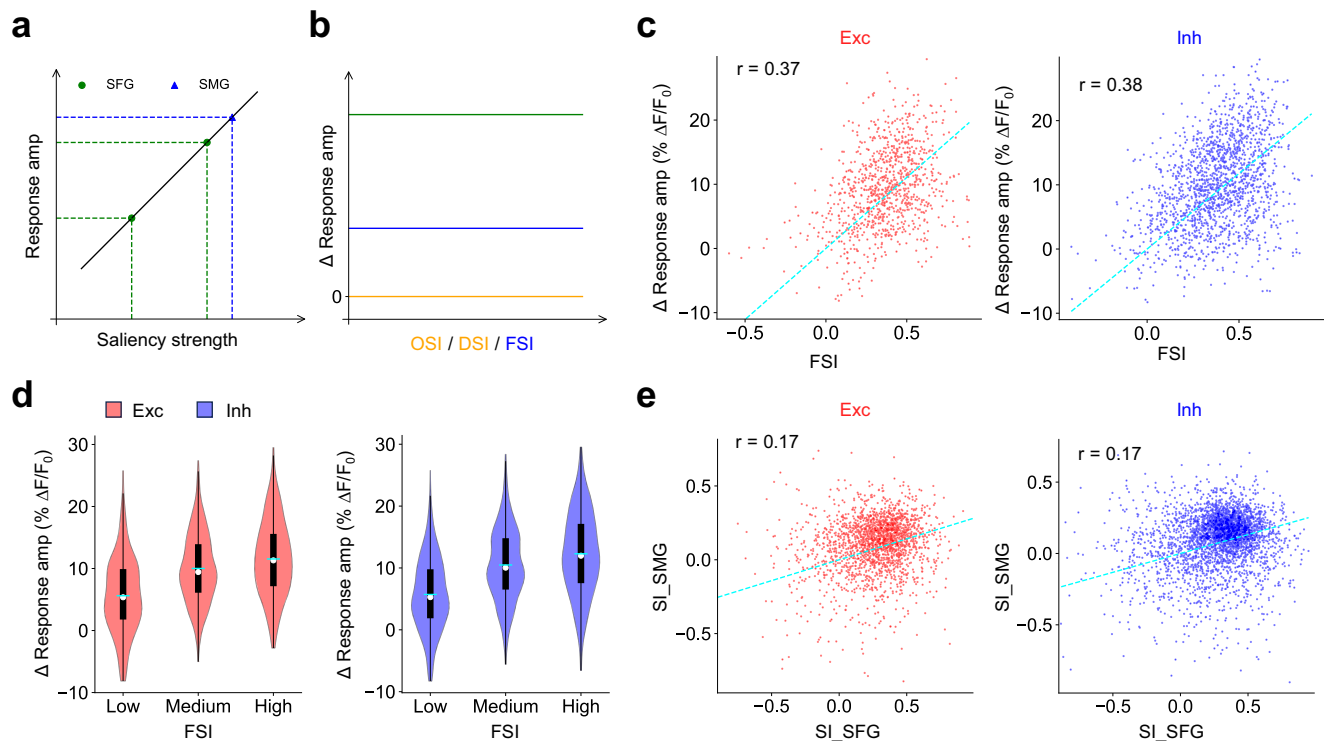


Fig. 5 | Encoding of visual saliency depends on the preference across different visual features. **a** Response amplitude as a function of saliency strength for ideal saliency-encoding neurons, independent of the preference for specific visual features. Green dots indicate response amplitude to SFGs with different orientation contrasts. The blue triangle indicates the response amplitude to SMG, which may be more or less salient than the SFG. **b** Response amplitude difference between two salient stimuli as a function of neurons' preferences for specific orientations, directions, and features. **c** Difference in response amplitude between SFG and SMG (SMG-SFG) versus FSI; r is Pearson's correlation coefficient: $p < 0.001$ for both

excitatory and inhibitory neurons. Exc: $N = 968$; Inh: $N = 1688$. Cyan lines represent linear fits. **d** Violin plots for the difference in response amplitudes evoked by SFGs and SMGs for saliency-encoding neurons across different levels of feature selectivity. Low: $FSI < 0.25$; Medium: $0.25 \leq FSI < 0.5$; $FSI \geq 0.5$. One-way ANOVA, $p < 0.001$ for both excitatory and inhibitory neurons; $p < 0.001$ for all pairwise comparisons using Tukey's range test. Exc: $N = 270, 484, 248$; Inh: $N = 651, 1272, 713$. **e** SI_SMG is positively correlated with SI_SFG: r is Pearson's correlation coefficient, $p < 0.001$ for both excitatory and inhibitory neurons. Exc: $N = 2056$; Inh: $N = 3344$.

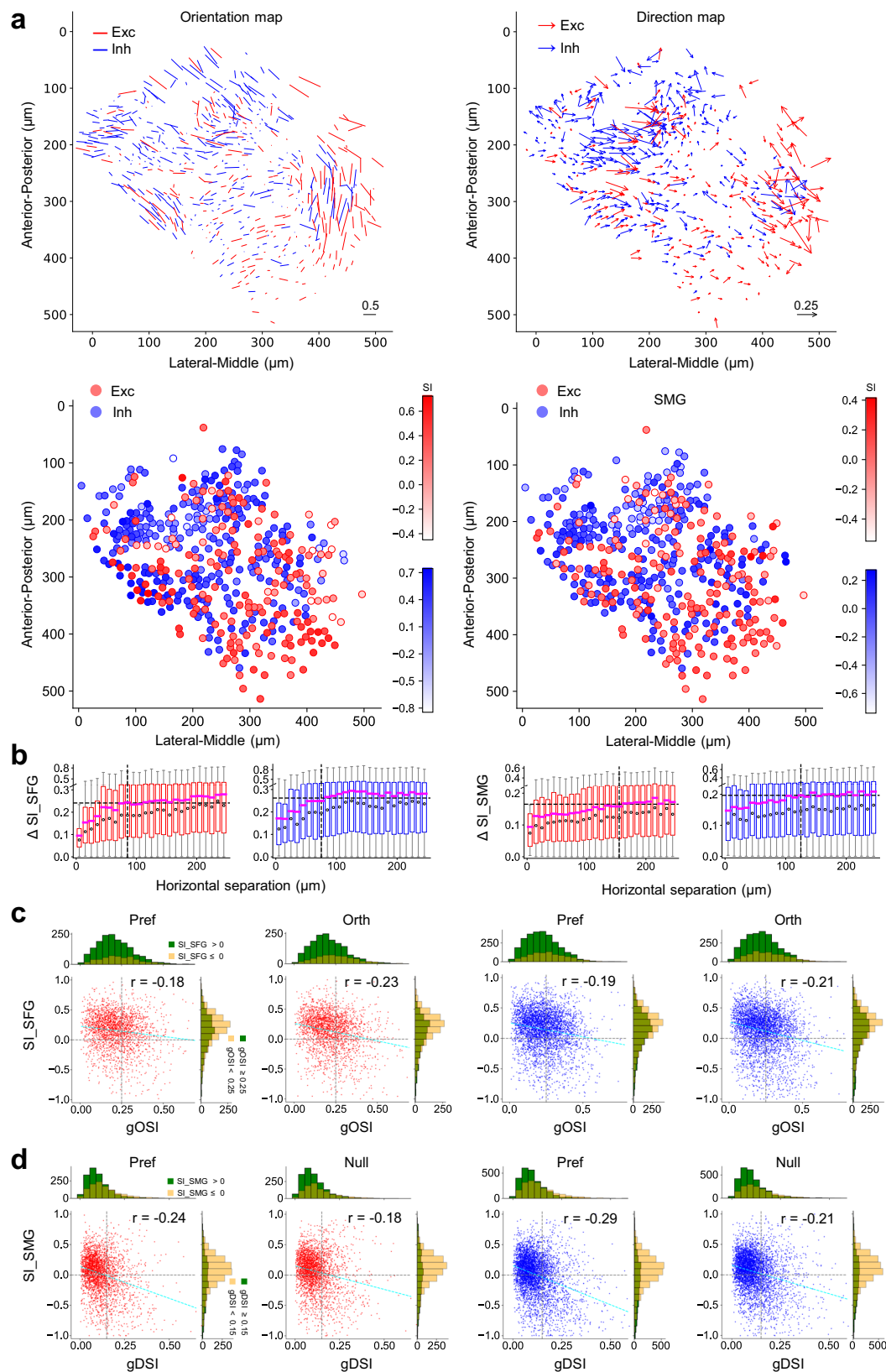
Discussion

Cracking the neural encoding of visual saliency is important for understanding how useful information is extracted from massive visual input—a process critical for animals to survive and thrive in complex and dynamic environments. To uncover how visual saliency is encoded in the sSC, we applied two-photon calcium imaging to measure the responses of excitatory and inhibitory neurons to salient visual stimuli in awake mice. We found that excitatory and inhibitory neurons show similar response properties to these stimuli (Fig. 1). Specifically, salient stimuli evoke the strongest responses when centered in the RF, with response amplitudes gradually declining as the stimuli move away up to $\sim 40^\circ$ (Figs. 2 and 3). Notably, the response amplitude to salient stimuli is independent of the neurons' orientation and direction preference (Figs. 2 and 3); instead, it is determined by the saliency strength of the stimuli (Fig. 4). However, comparing neuronal responses to salient stimuli made by orientation versus motion direction reveals that response amplitudes are influenced by feature preference (Fig. 5). Further analysis reveals that saliency-encoding neurons are less tuned to orientation and motion direction and form saliency maps (Fig. 6). Notably, preference-independent saliency encoding in the sSC persists after removing cortical inputs (Fig. 7). These findings provide partial support for the saliency encoding theory proposed by Koch and Ullman⁸.

Our findings align with and extend previous studies on the factors influencing neuronal responses to salient stimuli in the sSC. First, the size of the salient stimulus plays a role. In our study, sSC neurons exhibit maximal responses to a 10° salient stimulus presented at the RF center, but the stimulus edge also elicits stronger responses than the background. As the stimulus size increases beyond the RF size, iso-feature suppression reduces responses to the stimulus center, causing neurons to function as edge

detectors⁴⁴. Second, neuronal responses are influenced by anesthesia. In anesthetized mice, excitatory neurons in the sSC show stronger responses to motion contrast relative to the background, while inhibitory neurons show weaker responses. Both neuron types, however, respond more strongly to orientation contrast²⁶. In contrast, our findings in awake mice reveal that excitatory and inhibitory neurons respond similarly to salient stimuli induced by orientation or motion direction. Third, saliency encoding in the sSC does not require cortical inputs. While previous work reported that V1 limits saliency encoding in the sSC²⁷, our findings show that this limitation was observed in both excitatory and inhibitory neurons. Moreover, the preference-independence property of saliency encoding does not require cortical inputs. Finally, our findings are not influenced by the sharp edges in square patches with square gratings, as consistent results were obtained using circular patches with sinusoidal gratings (Supplementary Figs. 4 and 5).

While both V1 and SC show stronger responses to salient stimuli compared to iso-feature backgrounds, previous studies indicate distinct mechanisms of saliency encoding between these two regions. In primate V1, neurons exhibit strong preferences for specific orientations or motion directions⁴⁵, and the encoding of visual saliency is closely tied to these preferences^{13–15}. For example, when the orientation surrounding a neuron's RF matches its preferred orientation, iso-orientation stimuli within the RF elicit stronger responses than cross-orientation stimuli. Conversely, when the surrounding orientation is orthogonal to the neuron's preferred orientation, cross-orientation stimuli become more effective. These contextual effects can be understood by convolving the visual stimulus with the neuron's subthreshold RF (Supplementary Fig. 8), which reflects integrated synaptic inputs and is larger than the spike RF⁴⁶. However, it remains to be



determined whether these findings generalize to mouse V1, where neurons respond robustly to salient stimuli⁴⁷ but show weaker orientation selectivity compared to cats and monkeys^{48–50}.

In contrast, neurons in the primate sSC are less tuned to specific orientations or motion directions but show robust responses to salient

locations in natural scenes^{16,51,52}, suggesting a feature-agnostic encoding of saliency. This aligns with observations in the rat sSC, where visual saliency encoding is not influenced by orientation preference⁵³. Similarly, in the optic tectum, the non-mammalian homologue of SC, neurons encode direction-induced visual saliency in a preference-independent manner^{54–56}. Our

Fig. 6 | Saliency-encoding neurons are less selective to orientation and motion direction. **a** Upper panels: orientation map and direction map represented by excitatory and inhibitory neurons in an example imaging plane. The length of lines or arrows is proportional to gOSI or gDSI. Lower panels: saliency maps measured by SFGs and SMGs in the same plane. **b** Box plots for the absolute difference in SI of neuron pairs versus their horizontal distance. Black dashed lines indicate the separation at 75% of the maximum. SFG_Exc: 85 μm , $N = 167834$ neuron pairs; SFG_Inh: 75 μm , $N = 400335$ neuron pairs; SMG_Exc: 155 μm , $N = 167834$ neuron

pairs; SMG_Inh: 125 μm , $N = 400335$ neuron pairs. c SI is negatively correlated with gOSI measured by flashing gratings: r is Pearson's correlation coefficient, $p < 0.001$ for all panels. Top inset: histograms of gOSI for neurons with $\text{SI} < 0$ and $\text{SI} \geq 0$. Right inset: histograms of SI for neurons with $\text{gOSI} < 0.25$ and $\text{gOSI} \geq 0.25$. **d** SI is negatively correlated with gDSI measured by moving gratings: $p < 0.001$ for all panels. Top inset: histograms of gDSI for neurons with $\text{SI} < 0$ and $\text{SI} \geq 0$. Right inset: histograms of SI for neurons with $\text{gDSI} < 0.15$ and $\text{gDSI} \geq 0.15$.

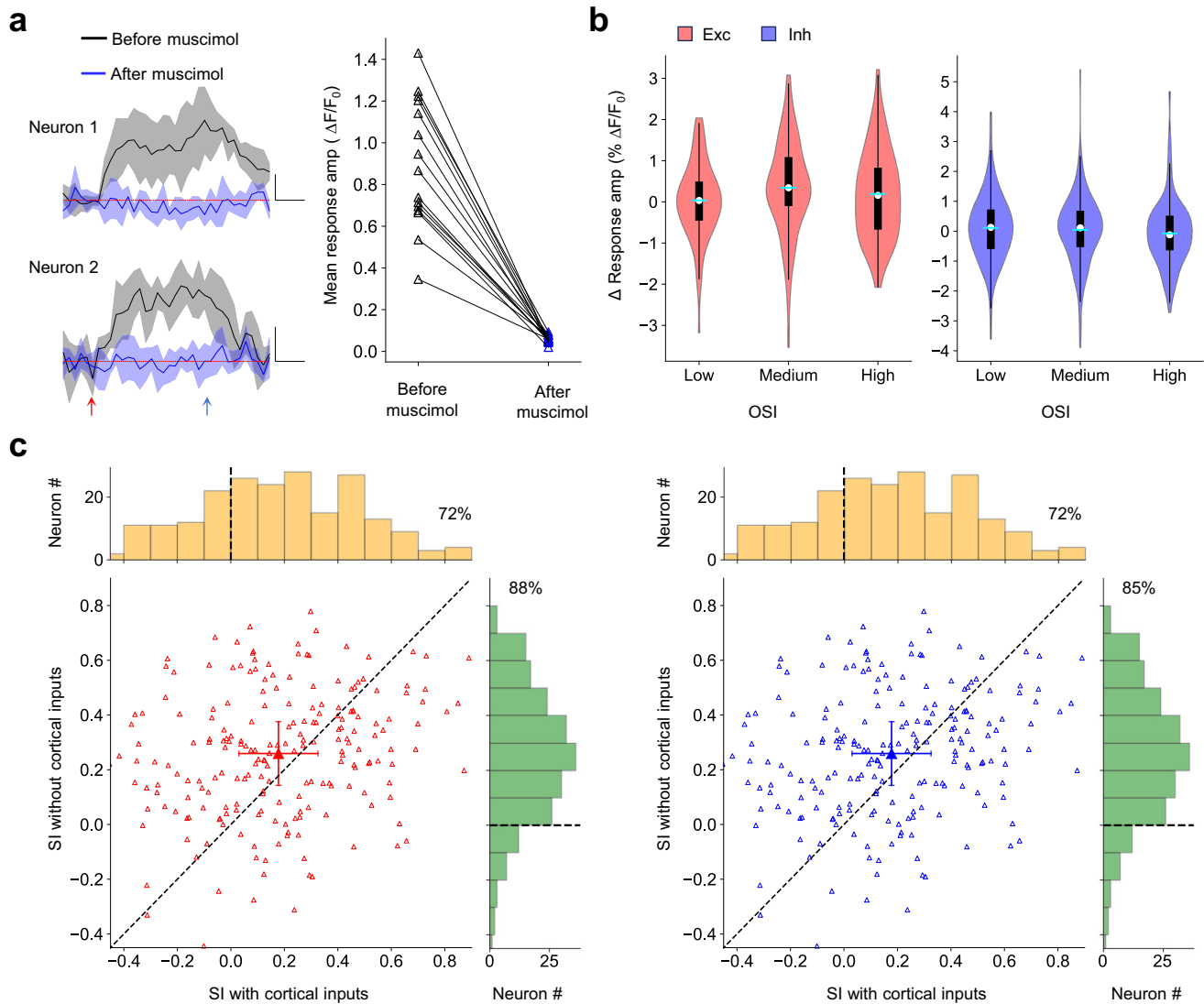


Fig. 7 | Preference-independent saliency encoding in the sSC does not require cortical inputs. **a** Two examples and the summary of visually evoked neuronal responses in V1 before and after muscimol injections. Gray shade indicates the SD across 5 trials. Blue and red arrows mark the onset and offset of visual stimuli, respectively. Red lines indicate the baseline activity without visual stimulation. Scales: 30% $\Delta F/F_0$, 0.5 s. $N = 15$ neurons. **b** Violin plots for the difference in response amplitudes evoked by SFGs with preferred and orthogonal backgrounds for saliency-encoding neurons across different levels of orientation selectivity after

cortical silencing. The means of the three groups are the same: one-way ANOVA, $p = 0.19$ for excitatory neurons, $N = 84, 74, 50$; $p = 0.41$ for inhibitory neurons, $N = 163, 156, 112$. c SI of excitatory and inhibitory neurons in the sSC without versus with cortical inputs. Exc: 0.18 ± 0.30 vs. 0.26 ± 0.23 , $N = 208$; Inh: 0.18 ± 0.29 vs. 0.24 ± 0.23 , $N = 431$. Black dashed lines indicate the identity line. Error bars represent standard deviation. Top and right insets: histograms of SI with and without cortical inputs. Black dashed lines mark SI = 0. Percentage values indicate the proportion of neurons with SI > 0.

findings in the mouse SC provide further evidence that saliency encoding in the sSC is independent of both orientation and direction preferences, supporting a general principle of saliency encoding across species.

How is the saliency map implemented in the sSC? As proposed in the computational model, surrounding inhibition is essential for generating the saliency map^{8,9}. Compared to V1, sSC contains a larger proportion of

inhibitory neurons. These inhibitory neurons have horizontally extended dendritic arbors that span up to 500 μm , accounting for ~60% of all neurons in the sSC^{38,42}. In contrast, inhibitory neurons in V1 exhibit heterogeneous morphologies and represent only ~25% of the total neuronal population⁵⁷. Another contributing factor is the functional patches in the sSC^{33,36}. The size of these patches is comparable to the observed long-range effect over ~40°

(Figs. 2c and 3b), and the connection strength between neurons is affected by both their distance and functional similarity^{58–60}. Furthermore, wide-field excitatory neurons with large dendrites may also play a role in saliency encoding⁴².

Alternatively, the saliency map could be inherited from the retina or V1. In the retina, salient stimuli made by orientation or motion direction elicit stronger responses in retinal ganglion cells (RGCs) compared to uniform stimuli^{61,62}. Importantly, object motion sensitive RGCs respond robustly to salient moving stimuli independently of their direction preferences^{63,64}, suggesting that saliency encoding in sSC may be partially inherited from the retina. In contrast, cortical inputs from V1 reduce the distinction between responses evoked by cross-orientation and iso-orientation stimuli, thereby compromising the encoding capacity²⁷. Future modeling work could explore how these factors collectively contribute to the preference-independent saliency map in the sSC.

What is the role of SC in visual attention? In primates, the sSC plays a critical role in bottom-up attention but does not participate in arousal-related top-down attention^{16,20}. Supporting this, our data show that saliency encoding is not affected by pupil size (Supplementary Fig. 1e), a well-established indicator of arousal state⁶⁵. The sSC projects to multiple brain regions, including the pulvinar, the lateral geniculate nucleus, and the iSC^{42,66}. The iSC plays a key role in top-down attention, receiving direct inputs from the prefrontal cortex⁶⁷. It encodes learned saliency relevant to behavioral tasks¹⁶ and integrates sensory information from different modalities⁶⁸. These properties position the iSC as an ideal hub for integrating the preference-independent saliency map from sSC with goal-driven attention, ultimately generating a modality-independent priority map that determines the attended location. Indeed, inactivating the deep layers of the primate SC impairs behavioral performance in visual attention tasks⁶⁹. An exciting direction for future research is to explore how the preference-independent visual saliency map in the sSC is transformed into the modality-independent priority map in the iSC.

Beyond physical differences or learned associations, visual saliency can also arise from ethological relevance—stimuli that are inherently significant due to evolutionary pressures. For example, looming stimuli, which signal the approach of a predator, naturally capture an animal's attention. Recent studies in mice have demonstrated that both sSC and iSC are more strongly activated by such ethologically relevant stimuli compared to neutral ones^{36,70–73}. These findings indicate that the SC is involved in three types of saliency: physical saliency based on contrast, ethological saliency shaped by evolution, and learned saliency derived from experience. Understanding how these types of saliency are encoded, integrated, and interact in the brain could provide insights into the neural mechanisms that underlie attention and decision-making.

Methods

All experimental procedures were performed under animal welfare guidelines and approved by the Institutional Animal Care and Use Committee at the Chinese Institute for Brain Research, Beijing. We have complied with all relevant ethical regulations for animal use.

Animal

Vglut2-ires-Cre (JAX no. 028863) or Vgat-ires-Cre (JAX no. 028862) mice were crossed with Ai14 mice (JAX no. 007914) to express tdTomato in either excitatory (Vglut2+) or inhibitory (Vgat+) neurons. A total of nine mice at ages 2–4 months were used: one male and two female Vglut2-tdTomato mice, and five female Vgat-tdTomato mice. In addition, one male Thy1-GCaMP6s (GP3.4, JAX no. 024275) mouse was used for cortical imaging.

Viral injection and plug implantation

Adeno-associated viruses expressing non-floxed GCaMP8m (AAV2/9-syn-jGCaMP8m-WPRE, 1×10^{13} GC/ml dissolved in $1 \times$ PBS) were

injected into the SC of Vglut2-tdTomato and Vgat-tdTomato mice. The injection coordinates were 0.42 mm anterior and 0.5 mm lateral to the lambda, at two depths of 1.0 mm and 1.6 mm. At each depth, 200 nl of AAVs were injected at a speed of 50 nl/min, followed by a 5-min waiting period before slowly retracting the pipette. After three weeks, a custom-made head plate was attached to the skull and a silicon plug was implanted. Specifically, a 3 mm \times 2 mm oval craniotomy was made 0.5 mm posterior to the lambda, and the dura was removed. The silicone plug was placed posterior to the transverse sinus and pushed forward \sim 1 mm to expose the posterior-medial portion of the sSC, which corresponds to the upper-temporal region of visual field. Three days after implantation, two-photon microscopy was used to image calcium signals in the sSC of head-fixed awake mice.

In vivo two-photon calcium imaging

Mice were head-fixed on a treadmill and allowed to move freely. After a 15-min habituation period, two-photon imaging was performed using an Ultima 2P Plus microscope (Bruker) with a 16 \times , 0.8 NA, 3-mm WD objective (CF175, Nikon). A tunable femtosecond laser (InSight X3+ Dual, Spectra-Physics) was raster-scanned using resonant galvanometers. GCaMP8m and tdTomato were excited at 920 nm, with laser power at the sample plane typically set between 30 and 50 mW. For each session, three 550 μ m \times 550 μ m fields of view (FOVs) were imaged at different depths, spaced 50 μ m apart. Each FOV was captured as 512 \times 512 pixel images with a sampling rate of 10 Hz, with imaging depths up to 350 μ m. Emitted green and red fluorescence were split with a dichroic mirror (t565lpxr), passed through two bandpass filters (et525/70m-2p and et595/50m-2p), and detected by two GaAsP photomultiplier tubes (H10770PB-40, Hamamatsu). The animal's locomotion, pupil size, and pupil position were recorded and synchronized with image acquisition. During imaging sessions, mice exhibited rare eye movements and locomotion.

Visual stimulation

A 21-inch LED monitor was placed 17 cm away from the mouse's right eye, centered at 95° azimuth and 25° elevation, covering a 104° \times 80° visual field. During the habituation period, the screen displayed a gray background. To locate the receptive field (RF) of recorded neurons, for each imaging session, we manually moved a 10° black or white dot across the screen and identified a 40° \times 60° responsive region. To investigate how visual saliency is encoded in the sSC, we presented six types of visual stimuli. (1) A 4 \times 6 grid of 10° \times 10° flashing squares (one at a time, 1 s black or white + 1 s gray) in this identified region to map the RF. (2) A full-field flashing square or sinusoidal grating (0.1 cycles/degree spatial frequency, 1 Hz temporal frequency, 4 s grating + 1 s gray) presented in 6 orientations and 4 phases to measure the orientation selectivity. (3) a grid of 4 \times 6 grid of 10° \times 10° flashing square patches with square gratings or 10° circle patches with sinusoidal gratings in vertical (0°) or horizontal (180°) orientations on a full-field grating background in the orthogonal orientation. (4) A 10° \times 10° flashing square patch with square gratings or a 10° circle patch with sinusoidal gratings in 6 orientations presented at the center of the identified region on a vertical or horizontal grating background. (5) A full-field moving square or sinusoidal gratings (0.1 cycles/degree spatial frequency, 1 Hz temporal frequency, 2 s grating + 1 s gray) presented in 12 directions to measure the direction selectivity. (6) a 4 \times 6 grid of 10° \times 10° moving square patches with square gratings or 10° circle patches with sinusoidal gratings moving in 0°, 90°, 180°, and 270° directions on a full-field grating background moving in the opposite directions. All stimuli were displayed for 5 repetitions, and the sequence was pseudo-randomized for each stimulus.

Cortical silencing

To assess the cortical influence on saliency encoding in the sSC, we measured the responses of SC neurons to salient stimuli before and after

cortical silencing. V1 was silenced with muscimol, a GABA_A receptor agonist. A 3-mm coverslip was implanted 0.5 mm anterior and 2.5 mm lateral to the lambda, targeting the V1 region that corresponds to the upper-temporal visual field. The coverslip had a 0.6 mm hole in the center for drug delivery. We first imaged neuronal responses in the sSC and then injected 150 nl of 5 mM muscimol (Sigma-Aldrich) at a depth of 0.4 mm using a micro-injection pipette. The injection process lasted about 5 min. After a 30-min waiting period to allow the drug to take effect, we re-imaged visually evoked responses in the same imaging plane. To confirm cortical silencing, we performed two-photon calcium imaging of cortical neurons, measuring their responses to moving sinusoidal gratings before and after injection.

Data analysis

Measurement of calcium responses. Brain motion during the imaging was corrected using NoRMCorre⁷⁴ and CalmAm⁷⁵. Regions of interest (ROIs) were manually drawn using the Cell Magic Wand Tool (ImageJ) and fitted with an ellipse. Fluorescence traces for each ROI were extracted after estimating and removing contamination from surrounding neuropil signals, as described previously^{36,76,77}. The true fluorescence signal of a neuron was calculated as $F_{true} = F_{raw} - (r \cdot F_{neuropil})$, where r is the out-of-focus neuropil contamination factor, estimated to be ~ 0.7 for our setup. Slow baseline fluctuations were removed using detrended fluctuation analysis with a 15-s sliding window.

For any given stimulus, the neuronal response was defined by the fluorescence trace in its ROI during the stimulus period:

$$R = \frac{F - F_0}{F_0} \tag{1}$$

where F is the instantaneous fluorescence intensity, and F_0 is the mean fluorescence intensity without visual stimulation (gray screen).

Two criteria were applied to interpret ROIs as neurons: (1) The ROI size was limited to 10–20 μm to match the typical size of a neuron; (2) The ROI response had to exceed a signal-to-noise ratio (SNR) of 0.5 for at least one visual stimulus⁴¹:

$$SNR = \frac{\text{Var}[\langle C \rangle_r]_t}{\langle \text{Var}[C]_r \rangle_t} \tag{2}$$

where C is the N_t (time samples) \times N_r (stimulus repetitions) response matrix, $t = 1, \dots, N_t$ and $r = 1, \dots, N_r$, $\langle \cdot \rangle_r$ and $\langle \cdot \rangle_t$ are the means over repetitions or time respectively, and $\text{Var}[\cdot]_r$ and $\text{Var}[\cdot]_t$ are the corresponding variances. All ROIs meeting these criteria were selected for further analysis, yielding a total of 8335 neurons, including 3232 excitatory neurons and 5103 inhibitory neurons.

Quantification of neuronal responses. To quantify orientation tuning, we calculated the orientation selectivity index (OSI) as the normalized difference between the response amplitude at the preferred and orthogonal orientations. The global orientation selectivity index (gOSI) was calculated as the normalized amplitude of the response-weighted vector sum across all orientations:

$$OSI = \frac{R(pref) - R(orth)}{R(pref) + R(orth)} \tag{3}$$

where $R(pref)$ and $R(orth)$ are the average responses to the preferred and orthogonal orientation, respectively.

$$gOSI = \frac{|\sum_k R(\theta_k) \times e^{2i\theta_k}|}{\sum_k R(\theta_k)} \tag{4}$$

where θ_k is the k^{th} orientation in radians, and $R(\theta_k)$ is the average response during the stimulus period at that orientation.

To quantify motion direction tuning, we calculated the DSI as the normalized difference between the response amplitude at the preferred and null directions. The global direction selectivity index (gDSI) was calculated as the normalized amplitude of the response-weighted vector sum of all directions:

$$DSI = \frac{R(pref) - R(null)}{R(pref) + R(null)} \tag{5}$$

where $R(pref)$ $R(null)$ are the average responses to the preferred or null direction, respectively.

$$gDSI = \frac{|\sum_k R(\rho_k) \times e^{i\rho_k}|}{\sum_k R(\rho_k)} \tag{6}$$

where ρ_k is the k^{th} direction in radians, and $R(\rho_k)$ is the average response during the stimulus period at that direction.

To quantify preference for salient stimuli, we calculated the SI as the relative difference between the response to SFGs or SMGs and the response to the background:

$$SI = \frac{R(s) - R(bg)}{R(s) + R(bg)} \tag{7}$$

where $R(s)$ is the average response to salient stimuli, and $R(bg)$ is the average response to the background.

To quantify preference for specific visual features, we calculated the FSI as the relative difference between the responses to flashing and moving gratings:

$$FSI = \frac{R(fg) - R(mg)}{R(fg) + R(mg)} \tag{8}$$

where $R(fg)$ is the average response to flashing gratings at the preferred orientation, and $R(mg)$ is the average response to moving gratings at the preferred motion direction.

To quantify RF properties, calcium responses at 4×6 spatial locations were fitted with a 2D Gaussian function:

$$f = A \cdot e^{-\frac{((x-E)\cos(D)-(y-F)\sin(D))^2}{2B^2} - \frac{((x-E)\sin(D)+(y-F)\cos(D))^2}{2C^2}} + G \tag{9}$$

The RF size is defined as the area at half maximum: $\pi \cdot 2 \ln 2 \cdot B \cdot C$. Subsequent analyses were omitted if the coefficient of determination for the fit was below 0.5. The RF center was also calculated as the center of mass for evoked responses, yielding consistent results with the Gaussian fitting.

Neural modeling

For simplicity, the model was built in 1D visual space with only two stimuli: positive and negative. Functional patches are simulated with a sinusoidal function, termed the functional preference index (FPI), which quantifies the preference of each neuron at different spatial locations. Since OSI is mainly correlated with responses at the orthogonal orientation (Supplementary Fig. 7d), we set a neuron’s response amplitude to its preferred stimulus as 1, while responses to non-preferred stimuli varied with FPI.

$$FPI = \cos(\pi/\rho * \mathbf{v}) \tag{10}$$

where $\rho = 30^\circ$ denotes the patch size^{33,36}, and \mathbf{v} is a vector representing the visual space (-60° to 60°).

The RF of each neuron was simulated as a 1D Gaussian function:

$$\text{RF} = \exp\left(-\frac{(\mathbf{v} - \boldsymbol{\mu})^2}{2\sigma^2}\right) \quad (11)$$

where $\boldsymbol{\mu}$ is the location of the RF center in visual space, and σ was set to 5° for the subthreshold RF.

The neuronal response to a given visual stimulus is simulated by convolving the RF with the stimulus.

$$R = R_p \times (\text{RF} \cdot \mathbf{vp}) + R_n \times (\text{RF} \cdot \mathbf{vn}) \quad (12)$$

Where \mathbf{vp} and \mathbf{vn} are the positive and negative stimuli, and R_p and R_n are the response amplitude.

Statistics and reproducibility

The Kolmogorov–Smirnov test was used to assess the normality of data distributions. Parametric tests were applied to normally distributed data, while non-parametric tests were used for all other data. Statistical significance was defined as $p < 0.05$. Sample sizes were not predetermined by statistical methods but followed common practices in the field.

Reporting summary

Further information on research design is available in the Nature Portfolio Reporting Summary linked to this article.

Data availability

Data are available in a GitHub repository at https://github.com/yatangli/Wu_SaliencyMap_2025 and a Zenodo repository⁷⁸ at <https://zenodo.org/records/15086844>.

Code availability

Code is available in a GitHub repository at https://github.com/yatangli/Wu_SaliencyMap_2025 and a Zenodo repository⁷⁸ at <https://zenodo.org/records/15086844>.

Received: 25 September 2024; Accepted: 26 March 2025;

Published online: 04 April 2025

References

- Zheng, J. & Meister, M. The unbearable slowness of being: why do we live at 10 bits/s? *Neuron* **113**, 192–204 (2025).
- Li, Z. A new framework for understanding vision from the perspective of the primary visual cortex. *Curr. Opin. Neurobiol.* **58**, 1–10 (2019).
- Treisman, A. M. & Gelade, G. A feature-integration theory of attention. *Cogn. Psychol.* **12**, 97–136 (1980).
- Treisman, A. Preattentive processing in vision. *Comput. Vis. Graph. Image Process.* **31**, 156–177 (1985).
- Posner, M. I. Orienting of attention. *Q. J. Exp. Psychol.* **32**, 3–25 (1980).
- Joseph, J. S. & Optican, L. M. Involuntary attentional shifts due to orientation differences. *Percept. Psychophys.* **58**, 651–665 (1996).
- Parkhurst, D. J. & Niebur, E. Texture contrast attracts overt visual attention in natural scenes. *Eur. J. Neurosci.* **19**, 783–789 (2004).
- Koch, C. & Ullman, S. Shifts in selective visual attention: towards the underlying neural circuitry. *Hum. Neurobiol.* **4**, 219–227 (1985).
- Itti, L., Koch, C. & Niebur, E. A model of saliency-based visual attention for rapid scene analysis. *IEEE Trans. Pattern Anal. Mach. Intell.* **20**, 1254–1259 (1998).
- Serences, J. T. & Yantis, S. Selective visual attention and perceptual coherence. *Trends Cogn. Sci.* **10**, 38–45 (2006).
- Fecteau, J. H. & Munoz, D. P. Saliency, relevance, and firing: a priority map for target selection. *Trends Cogn. Sci.* **10**, 382–390 (2006).
- Zhang, X., Zhaoping, L., Zhou, T. & Fang, F. Neural activities in V1 create a bottom-up saliency map. *Neuron* **73**, 183–192 (2012).
- Yan, Y., Zhaoping, L. & Li, W. Bottom-up saliency and top-down learning in the primary visual cortex of monkeys. *Proc. Natl. Acad. Sci.* **115**, 10499–10504 (2018).
- Knierim, J. J. & van Essen, D. C. Neuronal responses to static texture patterns in area V1 of the alert macaque monkey. *J. Neurophysiol.* **67**, 961–980 (1992).
- Sillito, A. M., Grieve, K. L., Jones, H. E., Cudeiro, J. & Davlis, J. Visual cortical mechanisms detecting focal orientation discontinuities. *Nature* **378**, 492–496 (1995).
- White, B. J. et al. Superior colliculus neurons encode a visual saliency map during free viewing of natural dynamic video. *Nat. Commun.* **8**, 14263 (2017).
- Mazer, J. A. & Gallant, J. L. Goal-related activity in V4 during free viewing visual search: evidence for a ventral stream visual salience map. *Neuron* **40**, 1241–1250 (2003).
- Gottlieb, J. P., Kusunoki, M. & Goldberg, M. E. The representation of visual salience in monkey parietal cortex. *Nature* **391**, 481–484 (1998).
- Thompson, K. G. & Bichot, N. P. A visual salience map in the primate frontal eye field. *Prog. Brain Res.* **147**, 251–262 (2005).
- Veale, R., Hafed, Z. M. & Yoshida, M. How is visual salience computed in the brain? Insights from behaviour, neurobiology and modelling. *Philos. Trans. R. Soc. B: Biol. Sci.* **372**, 20160113 (2017).
- Blakemore, C. & Tobin, E. A. Lateral inhibition between orientation detectors in the cat's visual cortex. *Exp. Brain Res.* **15**, 439–440 (1972).
- Kastner, S., Nothdurft, H.-C. & Pigarev, I. N. Neuronal responses to orientation and motion contrast in cat striate cortex. *Vis. Neurosci.* **16**, 587–600 (1999).
- Nothdurft, H.-C., Gallant, J. L. & Essen, D. C. V. Response modulation by texture surround in primate area V1: correlates of “popout” under anesthesia. *Vis. Neurosci.* **16**, 15–34 (1999).
- Jones, H. E., Grieve, K. L., Wang, W. & Sillito, A. M. Surround suppression in primate V1. *J. Neurophysiol.* **86**, 2011–2028 (2001).
- Jones, H. E., Wang, W. & Sillito, A. M. Spatial organization and magnitude of orientation contrast interactions in primate v1. *J. Neurophysiol.* **88**, 2796–2808 (2002).
- Barchini, J., Shi, X., Chen, H. & Cang, J. Bidirectional encoding of motion contrast in the mouse superior colliculus. *eLife* **7**, e35261 (2018).
- Ahmadlou, M., Tafreshiha, A. & Heimel, J. A. Visual cortex limits pop-out in the superior colliculus of awake mice. *Cereb. Cortex* **27**, 5772–5783 (2017).
- Blasdel, G. G. & Salama, G. Voltage-sensitive dyes reveal a modular organization in monkey striate cortex. *Nature* **321**, 579–585 (1986).
- Bonhoeffer, T. & Grinvald, A. Iso-orientation domains in cat visual cortex are arranged in pinwheel-like patterns. *Nature* **353**, 429–431 (1991).
- Malonek, D., Tootell, R. B. H. & Grinvald, A. Optical imaging reveals the functional architecture of neurons processing shape and motion in owl monkey area MT. *Proc. R. Soc. Lond. B* **258**, 109–119 (1994).
- Weliky, M., Bosking, W. H. & Fitzpatrick, D. A systematic map of direction preference in primary visual cortex. *Nature* **379**, 725–728 (1996).
- Ohki, K., Chung, S., Ch'ng, Y. H., Kara, P. & Reid, R. C. Functional imaging with cellular resolution reveals precise micro-architecture in visual cortex. *Nature* **433**, 597 (2005).
- Feinberg, E. H. & Meister, M. Orientation columns in the mouse superior colliculus. *Nature* **519**, 229–232 (2015).
- Ahmadlou, M. & Heimel, J. A. Preference for concentric orientations in the mouse superior colliculus. *Nat. Commun.* **6**, 6773 (2015).
- de Malmazet, D., Kühn, N. K. & Farrow, K. Retinotopic separation of nasal and temporal motion selectivity in the mouse superior colliculus. *Curr. Biol.* **28**, 2961–2969.e4 (2018).

36. Li, Y.-t., Turan, Z. & Meister, M. Functional architecture of motion direction in the mouse superior colliculus. *Curr. Biol.* **30**, 3304–3315.e4 (2020).
37. Li, Z., Wu, R. & Li, Y.-T. Calcium imaging in mouse superior colliculus. *J. Vis. Exp.* **194**, e65181(2023).
38. Liu, Y. et al. Mapping visual functions onto molecular cell types in the mouse superior colliculus. *Neuron* **111**, 1876–1886.e5 (2023).
39. Schröder, S. et al. Arousal modulates retinal output. *Neuron* **107**, 487–495.e9 (2020).
40. Wang, L., Sarnaik, R., Rangarajan, K., Liu, X. & Cang, J. Visual receptive field properties of neurons in the superficial superior colliculus of the mouse. *J. Neurosci.* **30**, 16573–16584 (2010).
41. Li, Y.-t. & Meister, M. Functional cell types in the mouse superior colliculus. *eLife* **12**, e82367 (2023).
42. Gale, S. D. & Murphy, G. J. Distinct representation and distribution of visual information by specific cell types in mouse superficial superior colliculus. *J. Neurosci.* **34**, 13458–13471 (2014).
43. Zhao, X., Liu, M. & Cang, J. Visual cortex modulates the magnitude but not the selectivity of looming-evoked responses in the superior colliculus of awake mice. *Neuron* **84**, 202–213 (2014).
44. Liang, Y., Lu, R., Borges, K. & Ji, N. Stimulus edges induce orientation tuning in superior colliculus. *Nat. Commun.* **14**, 4756 (2023).
45. Hubel, D. H. & Wiesel, T. N. Receptive fields and functional architecture of monkey striate cortex. *J. Physiol.* **195**, 215–243 (1968).
46. Li, Y.-t. et al. Broadening of inhibitory tuning underlies contrast-dependent sharpening of orientation selectivity in mouse visual cortex. *J. Neurosci.* **32**, 16466–16477 (2012).
47. Self, M. W. et al. Orientation-tuned surround suppression in mouse visual cortex. *J. Neurosci.* **34**, 9290–9304 (2014).
48. Niell, C. M. & Stryker, M. P. Highly selective receptive fields in mouse visual cortex. *J. Neurosci.* **28**, 7520–7536 (2008).
49. Tan, A. Y. Y., Brown, B. D., Scholl, B., Mohanty, D. & Priebe, N. J. Orientation selectivity of synaptic input to neurons in mouse and cat primary visual cortex. *J. Neurosci.* **31**, 12339–12350 (2011).
50. Van Hooser, S. D. Similarity and diversity in visual cortex: is there a unifying theory of cortical computation? *Neuroscientist* **13**, 639–656 (2007).
51. Chen, C.-Y. & Haged, Z. M. Orientation and contrast tuning properties and temporal flicker fusion characteristics of primate superior colliculus neurons. *Front. Neural Circuits* **12**, 58 (2018).
52. Goldberg, M. E. & Wurtz, R. H. Activity of superior colliculus in behaving monkey. I. Visual receptive fields of single neurons. *J. Neurophysiol.* **35**, 542–559 (1972).
53. Girman, S. V. & Lund, R. D. Most superficial sublamina of rat superior colliculus: neuronal response properties and correlates with perceptual figure-ground segregation. *J. Neurophysiol.* **98**, 161–177 (2007).
54. Frost, B. J. & Nakayama, K. Single visual neurons code opposing motion independent of direction. *Science* **220**, 744–745 (1983).
55. Sun, H.-J., Zhao, J., Southall, T. L. & Xu, B. Contextual influences on the directional responses of tectal cells in pigeons. *Vis. Neurosci.* **19**, 133–144 (2002).
56. Zahar, Y., Wagner, H. & Gutfreund, Y. Responses of tectal neurons to contrasting stimuli: an electrophysiological study in the barn owl. *PLoS ONE* **7**, e39559 (2012).
57. Markram, H. et al. Interneurons of the neocortical inhibitory system. *Nat. Rev. Neurosci.* **5**, 793–807 (2004).
58. Alonso, J.-M. & Martinez, L. M. Functional connectivity between simple cells and complex cells in cat striate cortex. *Nat. Neurosci.* **1**, 395–403 (1998).
59. Ko, H. et al. Functional specificity of local synaptic connections in neocortical networks. *Nature* **473**, 87–91 (2011).
60. Ts'o, D. Y., Gilbert, C. D. & Wiesel, T. N. Relationships between horizontal interactions and functional architecture in cat striate cortex as revealed by cross-correlation analysis. *J. Neurosci.* **6**, 1160–1170 (1986).
61. Girman, S. & Lund, R. Orientation-specific modulation of rat retinal ganglion cell responses and its dependence on relative orientations of the center and surround gratings. *J. Neurophysiol.* **104**, 2951–2962 (2010).
62. Chiao, C.-C. & Masland, R. H. Contextual tuning of direction-selective retinal ganglion cells. *Nat. Neurosci.* **6**, 1251–1252 (2003).
63. Baccus, S. A., Ölveczky, B. P., Manu, M. & Meister, M. A retinal circuit that computes object motion. *J. Neurosci.* **28**, 6807–6817 (2008).
64. Ölveczky, B. P., Baccus, S. A. & Meister, M. Segregation of object and background motion in the retina. *Nature* **423**, 401–408 (2003).
65. McGinley, M. J. et al. Waking state: rapid variations modulate neural and behavioral responses. *Neuron* **87**, 1143–1161 (2015).
66. May, P. J. The mammalian superior colliculus: laminar structure and connections. *Prog. Brain Res.* **151**, 321–378 (2006).
67. Hu, F. & Dan, Y. An inferior-superior colliculus circuit controls auditory cue-directed visual spatial attention. *Neuron* **110**, 109–119.e3 (2022).
68. Dräger, U. C. & Hubel, D. H. Physiology of visual cells in mouse superior colliculus and correlation with somatosensory and auditory input. *Nature* **253**, 203 (1975).
69. Zénon, A. & Krauzlis, R. J. Attention deficits without cortical neuronal deficits. *Nature* **489**, 434–437 (2012).
70. Wei, P. et al. Processing of visually evoked innate fear by a non-canonical thalamic pathway. *Nat. Commun.* **6**, 6756 (2015).
71. Shang, C. et al. A parvalbumin-positive excitatory visual pathway to trigger fear responses in mice. *Science* **348**, 1472–1477 (2015).
72. Lee, K. H., Tran, A., Turan, Z. & Meister, M. The sifting of visual information in the superior colliculus. *eLife* **9**, e50678 (2020).
73. Evans, D. A. et al. A synaptic threshold mechanism for computing escape decisions. *Nature* **558**, 590–594 (2018).
74. Pnevmatikakis, E. A. & Giovannucci, A. NoRMCorre: an online algorithm for piecewise rigid motion correction of calcium imaging data. *J. Neurosci. Methods* **291**, 83–94 (2017).
75. Giovannucci, A. et al. CalmAn an open source tool for scalable calcium imaging data analysis. *eLife* **8**, e38173 (2019).
76. Göbel, W. & Helmchen, F. In vivo calcium imaging of neural network function. *Physiology* **22**, 358–365 (2007).
77. Kerlin, A. M., Andermann, M. L., Berezovskii, V. K. & Reid, R. C. Broadly tuned response properties of diverse inhibitory neuron subtypes in mouse visual cortex. *Neuron* **67**, 858–871 (2010).
78. Li, Y.-t. & Wu, R. Preference-Independent Saliency Map in the Mouse Superior Colliculus [Data and code]. *Zenodo* <https://doi.org/10.5281/zenodo.15086844> (2025).

Acknowledgements

We thank the Laboratory Animal Resource Center, the Instrumental Core, and the Vector Core at CIBR for their service. We thank Dr. Tatsuo Okubo for commenting on the manuscript. Yatang Li is supported by the Natural Science Foundation of Beijing Municipality (IS23073), the National Natural Science Foundation of China (32271060), and the start-up fund from CIBR. Lingyun Li is supported by the Natural Science Foundation of Beijing Municipality (5244028) and the R&D Program of Beijing Municipal Education Commission (1240030201).

Author contributions

Ya-tang Li supervised the project; Ya-tang Li and Ruixiang Wu designed the experiments; Ruixiang Wu and Shu Lin collected the data; Ya-tang Li, Ruixiang Wu, Jinhui Xu, and Chunpeng Li analyzed the data; Ya-tang Li and Zhaoji Zhang carried out the neural modeling; Ruixiang Wu and Ya-tang Li prepared figures; Ya-tang Li and Lingyun Li wrote the manuscript.

Competing interests

The authors declare no competing interests.

Additional information

Supplementary information The online version contains supplementary material available at <https://doi.org/10.1038/s42003-025-08006-x>.

Correspondence and requests for materials should be addressed to Ya-tang Li.

Peer review information *Communications Biology* thanks Yu Gu, Lupeng Wang and the other, anonymous, reviewer(s) for their contribution to the peer review of this work. Primary Handling Editor: Jasmine Pan. A peer review file is available.

Reprints and permissions information is available at <http://www.nature.com/reprints>

Publisher's note Springer Nature remains neutral with regard to jurisdictional claims in published maps and institutional affiliations.

Open Access This article is licensed under a Creative Commons Attribution-NonCommercial-NoDerivatives 4.0 International License, which permits any non-commercial use, sharing, distribution and reproduction in any medium or format, as long as you give appropriate credit to the original author(s) and the source, provide a link to the Creative Commons licence, and indicate if you modified the licensed material. You do not have permission under this licence to share adapted material derived from this article or parts of it. The images or other third party material in this article are included in the article's Creative Commons licence, unless indicated otherwise in a credit line to the material. If material is not included in the article's Creative Commons licence and your intended use is not permitted by statutory regulation or exceeds the permitted use, you will need to obtain permission directly from the copyright holder. To view a copy of this licence, visit <http://creativecommons.org/licenses/by-nc-nd/4.0/>.

© The Author(s) 2025